Chapter

Boundary Element Modeling and Simulation Algorithm for Fractional Bio-Thermomechanical Problems of Anisotropic Soft Tissues

Mohamed Abdelsabour Fahmy

Abstract

The main purpose of this chapter is to propose a novel boundary element modeling and simulation algorithm for solving fractional bio-thermomechanical problems in anisotropic soft tissues. The governing equations are studied on the basis of the thermal wave model of bio-heat transfer (TWMBT) and Biot's theory. These governing equations are solved using the boundary element method (BEM), which is a flexible and effective approach since it deals with more complex shapes of soft tissues and does not need the internal domain to be discretized, also, it has low RAM and CPU usage. The transpose-free quasi-minimal residual (TFQMR) solver are implemented with a dual-threshold incomplete LU factorization technique (ILUT) preconditioner to solve the linear systems arising from BEM. Numerical findings are depicted graphically to illustrate the influence of fractional order parameter on the problem variables and confirm the validity, efficiency and accuracy of the proposed BEM technique.

Keywords: boundary element method, modeling and simulation algorithm, bio-heat transfer, fractional bio-thermomechanical problems, anisotropic soft tissues

1. Introduction

Human body is a complex thermal system, Arsene d'Arsonval and Claude Bernard have shown that the temperature difference between arterial blood and venous blood is due to oxygenation of blood [1]. A large number of research papers in bio-heat transfer over the past few decades have focused on an understanding of the impact of blood flow on the temperature distribution within living tissues. Pennes [2] was the first attempt to explain the temperature distribution in human tissue with blood flow effect. The improvement of numerical models for determination of temperature distribution in living tissues has been a topic of interest for numerous researchers. Askarizadeh and Ahmadikia [3] introduced analytical solutions for the transient Fourier and non-Fourier bio-heat transfer equations. Li et al. [4] studied the bio-thermomechanical interactions within the human skin in the context of generalized thermoelasticity.

Analytical solutions for the current problem [5, 6] are very difficult to obtain, so numerical methods have become the main way for solving these problems [7–10]. The boundary element method (BEM) [11–21] is one of the numerical methods used to solve the current general problem [22–31]. Generally, Laplace-domain fundamental solutions are easier to obtain than time-domain fundamental solutions for engineering and scientific problems [32, 33]. consequently, the BEM is very helpful for problems that did not have time-domain fundamental solutions, because it requires the Laplace-domain fundamental solutions of the problem's governing equations. So, BEM expands the range of engineering problems that can be solved with the classical time-domain BEM.

The main aim of this chapter is to propose a new boundary element fractional model for describing the bio-thermomechanical properties of anisotropic soft tissues. The dual reciprocity boundary element method has been used to solve the TWMBT for obtaining the temperature distribution, and then the BEM has been used to obtain the displacement and stress at each time step. The linear systems from BEM were solved by the TFQMR solver with the ILUT preconditioner which reduces the number of iterations and the total CPU time.

A brief summary of the chapter is as follows: Section 1 introduces the background and provides the readers with the necessary information to books and articles for a better understanding of bio-thermomechanical problems in anisotropic soft tissues Section 2 describes the BEM modeling of the bio-thermomechanical interactions and introduces the partial differential equations that govern its related problems. Section 3 outlines the dual reciprocity boundary element method (DRBEM) for temperature field. Section 4 discusses the convolution quadrature boundary element method (CQBEM) for poro-elastic field. Section 5 presents the new numerical results that describe the bio-thermomechanical problems in anisotropic soft tissues.

2. Formulation of the problem

Consider an anisotropic soft tissue in the Cartesian coordinate system $Ox_1x_2x_3$ as shown in **Figure 1**. It occupies the region $\Omega = \left\{(x_1, x_2, x_3) : 0 < x_1 < \underline{\alpha}, 0 < x_2 < \underline{\beta}, 0 < x_3 < \underline{\gamma}\right\}$ with boundary Γ that is subdivided into two non-intersective parts Γ_D and Γ_N.

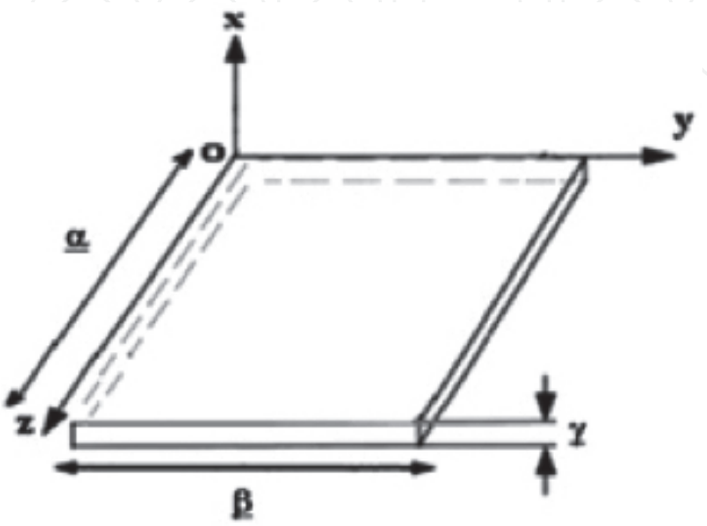

Figure 1.
Geometry of the current problem.

The governing equations which model the fractional bio-thermomechanical problems in anisotropic soft tissues can be written as follows [34, 35].

$$\left(\nabla^T \sigma\right)^T + F = \rho\ddot{u} + \phi\rho_f\left(\ddot{u}_f - \ddot{u}\right) \tag{1}$$

$$\dot{\zeta} + \nabla^T q = 0 \tag{2}$$

$$\sigma = \left(C_{ailg}\,\mathrm{tr}\in - Ap\right)I - \mathfrak{B}\theta, \tag{3}$$

$$\in = \frac{1}{2}\left(\nabla u^T + \left(\nabla u^T\right)^T\right) \tag{4}$$

$$\zeta = A\ \mathrm{tr}\in + \frac{\phi^2}{R}P \tag{5}$$

where the fluid was modeled by the following Darcy's law [36].

$$q = -K\left(\nabla p + \rho_f\ddot{u} + \frac{\rho_a + \phi\rho_f}{\phi}\left(\ddot{u}_f - \ddot{u}\right)\right) \tag{6}$$

The fractional order equation which describes the TWMBT can be expressed as [37].

$$\begin{aligned}&\nabla\mathcal{K}\nabla\mathcal{T}(r,\tau) + W_b C_b(\mathcal{T}_b - \mathcal{T}) + Q_{met} + Q_{ext} + \frac{\overline{\tau}}{\alpha!}\left(-W_b C_b D_\tau^\alpha\mathcal{T} + D_\tau^\alpha Q_{met} + D_\tau^\alpha Q_{ext}\right)\\ &= \rho C\left[\frac{\overline{\tau}}{\alpha!}D_\tau^{\alpha+1}\mathcal{T} + \frac{\partial\mathcal{T}}{\partial\tau}\right], 0 < \alpha \le 1\end{aligned} \tag{7}$$

where σ, $\in$, C_{ajlg}, $\rho = \rho_s(1-\phi) + \phi\rho_f$, ρ_s, ρ_f, u, u_f, FF and qq are total stress tensor, linear strain tensor, constant elastic moduli, bulk density, solid density, fluid density, solid displacement, fluid displacement, bulk body forces and specific flux of the fluid, respectively, $\mathfrak{B}$ are stress-temperature coefficients, tr denotes the trace, $A = \phi(1 + Q/R)$ is Biot's coefficient, Q and R are the solid–fluid coupling parameters, p is the fluid pressure in the vasculature, ζ is the fluid volume variation measured in unit reference volume, $\phi = \frac{V^f}{V}$ is the porosity, V^f is the fluid volume, $V = V^f + V^s$ is the bulk volume, V^s is the solid volume, τ is the time, K is the permeability, $\rho_a = \mathbb{C}\phi\rho_f$ where $\mathbb{C} = 0.66$ at low frequency [38], $\boldsymbol{K}$ is the soft tissue thermal conductivity, W_b is the blood perfusion rate, C_b is the blood specific heat, T_b is the arterial blood temperature, T is the soft tissue temperature, $\overline{\tau}$ is the thermal relaxation time ρ is the soft tissue density, C is the soft tissue specific heat, Q_{met} is the metabolic heat generation and Q_{ext} is the external heat generation.

According to Bonnet [39], our problem can be expressed as a matrix system as [40].

$$\left.\begin{aligned}&\hat{B}_{\tilde{x}}\hat{u}^g(\tilde{x}) = 0 \text{ for } \tilde{x}\in\Omega\\ &\hat{u}^g(x) = \hat{g}_D \text{ for } x\in\Gamma_D\\ &\hat{t}^g(x) = \hat{g}_N \text{ for } x\in\Gamma_N\end{aligned}\right\} \tag{8}$$

where

$$\hat{B}_{\tilde{x}} = \begin{bmatrix} B^e_{\tilde{x}} + s^2\left(\rho - \beta\rho_f\right)I & (\alpha-\beta)\nabla_{\tilde{x}} & -\mathfrak{B}\nabla_{\tilde{x}}\\ s(\alpha-\beta)\nabla^T_{\tilde{x}} & -\dfrac{\beta}{s\rho_f}\Delta_{\tilde{x}} + \dfrac{s\phi^2}{R} & 0\end{bmatrix} \tag{9}$$

$$\hat{t}^g(x) = \begin{bmatrix} T_x^e & -\alpha n_x & 0 \\ s\beta n_x^T & \dfrac{\beta}{s\rho_f} n_x^T \nabla_x & 0 \end{bmatrix} \begin{bmatrix} \hat{u}(x) \\ \hat{p}(x) \\ \theta(x) \end{bmatrix}, \quad \beta = \frac{\phi^2 sK\rho_f}{\phi^2 + sK\left(\rho_a + \phi\rho_f\right)} \tag{10}$$

3. Boundary element implementation for bioheat transfer field

Through this chapter, we supposed that Q_{met} and $\mathcal{T}_b$ are constants and $\theta(r,\tau) = \mathcal{T}(r,\tau) - \mathcal{T}(r,0)$. Thus, Eq. (7) can be written as

$$\rho C \frac{\overline{\tau}}{\alpha!} D_\tau^{\alpha+1}\theta + \rho C \frac{\partial\theta}{\partial\tau} + \frac{\overline{\tau}}{\alpha!} W_b C_b D_\tau^\alpha \theta + W_b C_b \theta = \mathcal{K}\frac{\partial^2\theta}{\partial x^2} + q, \quad 0 < \alpha \le 1 \tag{11}$$

According to finite difference scheme of Caputo [22] and using the fundamental solution of difference equation resulting from fractional bio-heat Eq. (11) [41], we can write the following dual reciprocity boundary integral equation

$$C_i\theta_i + \int_\Gamma q^*\theta d\Gamma - \int_\Gamma \theta^* q d\Gamma = \sum_{j=1}^{N+L} \alpha_j \left(C_j\hat{\theta}_{ij} + \int_\Gamma q^*\hat{\theta}_j d\Gamma - \int_\Gamma \theta^*\hat{q}_j d\Gamma \right) \tag{12}$$

in which

$$C_i = \frac{\gamma}{2\pi}, \quad q = \frac{\partial\theta}{\partial n}, \quad q^* = \frac{\partial\theta^*}{\partial n}, \quad \theta^* = \ln\left(\frac{1}{r}\right) \tag{13}$$

where n is the outward unit normal vector to boundary Γ, r is the distance between source point $\boldsymbol{i}$ and considered point j, N is the number of boundary nodes and L is the number of internal nodes.

where

$$\alpha = \mathbb{R}^{-1}\tilde{f} = \mathbb{R}^{-1}\left(\tilde{a}\frac{\partial^2\theta}{\partial\tau^2} + \tilde{b}\frac{\partial\theta}{\partial\tau} + \tilde{c}\theta + \tilde{d}\right) \tag{14}$$

The discretization process for Eq. (12) leads to

$$\begin{aligned} &C_i\theta_i + \sum_{k=1}^{N}\int_{\Gamma_k} q^*\theta d\Gamma - \sum_{k=1}^{N}\int_{\Gamma_k}\theta^* q d\Gamma \\ &= \sum_{j=1}^{N+L}\alpha_j\left(C_i\hat{\theta}_{ij} + \sum_{k=1}^{N}\int_{\Gamma_k} Z_{ik}\hat{\theta}_{kj}d\Gamma - \sum_{k=1}^{N}\int_{\Gamma_k} G_{ik}\hat{q}_{kj}d\Gamma \right) \end{aligned} \tag{15}$$

After interpolation and integration processes over boundary elements, Eq. (15) can be expressed as

$$C_i\theta_i + \sum_{k=1}^{N} Z_{ik}\theta_k - \sum_{k=1}^{N} G_{ik}q_k = \sum_{j=1}^{N+L}\alpha_j\left(C_i\hat{\theta}_{ij} + \sum_{k=1}^{N} Z_{ik}\hat{\theta}_{kj} - \sum_{k=1}^{N} G_{ik}\hat{q}_{kj} \right) \tag{16}$$

The matrix form of Eq. (16) can be written using (14) as

$$Z\theta - Gq = \left(Z\hat{\Theta} - G\hat{Q}\right)\mathbb{R}^{-1}\left(\tilde{a}\frac{\partial^2\theta}{\partial\tau^2} + \tilde{b}\frac{\partial\theta}{\partial\tau} + \tilde{c}\theta + \tilde{d}\right) \tag{17}$$

which also can be written

$$X\left(\tilde{a}\frac{\partial^2\theta}{\partial\tau^2}+\tilde{b}\frac{\partial\theta}{\partial\tau}+\tilde{c}\theta+\tilde{d}\right)+Z\theta=Gq \tag{18}$$

where

$$X=\left(Z\hat{\Theta}-G\hat{Q}\right)\mathbb{R}^{-1}$$

The boundary and initial conditions

$$\theta(x,y;\tau)=0 \tag{19}$$

$$\frac{\partial\theta(x,y;0)}{\partial\tau}=\vartheta(x,y;0)=0 \tag{20}$$

$$\theta(x,y;0)=\begin{cases}1^{\circ}\mathrm{C} & -0.02\le x,y\le 0.02\\ 0 & \text{other } x,y\end{cases} \tag{21}$$

The time discretization has been performed as follows

$$q=(1-\theta_q)q^m+\theta_q q^{m+1} \tag{22}$$

$$\theta=(1-\theta_u)\theta^m+\theta_u\theta^{m+1} \tag{23}$$

$$\frac{\partial\theta}{\partial\tau}=\frac{1}{\Delta\tau}\left(\theta^{m+1}-\theta^m\right) \tag{24}$$

$$\frac{\partial^2\theta}{\partial\tau^2}=\frac{1}{\Delta\tau^2}\left(\theta^{m+1}+\theta^{m-1}-2\theta^m\right) \tag{25}$$

Substituting from Eqs. (22)–(25) into (20), we obtain

$$\begin{aligned}&\left(\frac{X\tilde{a}}{\Delta\tau^2}+\frac{X\tilde{b}}{\Delta\tau}+X\tilde{c}\theta_u+\theta_u Z\right)\theta^{m+1}-\theta_q Gq^{m+1}+X\tilde{d}\\&=\left(\frac{2X\tilde{a}}{\Delta\tau^2}+\frac{X\tilde{b}}{\Delta\tau}-X\tilde{c}(1-\theta_u)-Z(1-\theta_u)\right)\theta^m-\frac{X\tilde{a}}{\Delta\tau^2}\theta^{m-1}+(1-\theta_q)Gq^m\end{aligned} \tag{26}$$

Thus, with the temperature θ determined, the remaining task is to solve the problem (8).

4. Boundary element implementation for the poro-elastic fields

The representation formula of (8) that describes the unknown field $\hat{u}^g$ can be written as

$$\hat{u}^g(\tilde{x})=\left(\hat{V}\hat{t}^g\right)_{\Omega}(\tilde{x})-\left(\hat{K}\hat{u}^g\right)_{\Omega}(\tilde{x}) \text{ for } \tilde{x}\in\boldsymbol{\Omega} \tag{27}$$

where

$$\left(\hat{V}\hat{t}^g\right)_{\Omega}(\tilde{x})=\int_{\dot{\Gamma}}\hat{U}^T(y-\tilde{x})\hat{t}^g(y)ds_y \tag{28}$$

$$\left(\hat{K}\hat{u}^g\right)_\Omega(\tilde{x}) = \int_\Gamma \left(\hat{T}_y\hat{U}\right)^T(y-\tilde{x})\hat{u}^g(y)ds_y \tag{29}$$

For anisotropic case, the Laplace domain fundamental solution $\hat{U}(r)$ and the corresponding traction $\hat{T}_v$ can be expressed as [40].

$$\hat{U}(r) = \begin{bmatrix} \hat{U}^s(r) & \hat{U}^f(r) & 0 \\ \left(\hat{P}^s\right)^T(r) & \hat{P}^f(r) & 0 \end{bmatrix}, \quad \hat{T}_y = \begin{bmatrix} T_y^e & san_y & 0 \\ -\beta n_y^T & \dfrac{\beta}{s\rho^f} n_y^T\nabla & 0 \end{bmatrix} \text{ with } r := |y-x| \tag{30}$$

where the solid displacement fundamental solution $\hat{U}^s(r)$ may be expressed as

$$\hat{U}^s(r) = \frac{1}{4\pi r(\rho-\beta\rho^f)}\left[\mathbb{R}_1\frac{(k_4^2-k_2^2)}{(k_1^2-k_2^2)}e^{-k_1 r} - \mathbb{R}_2\frac{(k_4^2-k_1^2)}{(k_1^2-k_2^2)}e^{-k_2 r} + \left(Ik_3^2-\mathbb{R}_3\right)e^{-k_3 r}\right] \tag{31}$$

with

$$\mathbb{R}_j = \frac{3\nabla_y r\nabla_y^T r - I}{r^2} + k_j\frac{3\nabla_y r\nabla_y^T r - I}{r} + k_j^2\nabla_y r\nabla_y^T r \tag{32}$$

which can be expressed as [36].

$$\hat{U}^s(r) = \frac{1}{4\pi\mu r(\lambda+2\mu)}\left[(\lambda+\mu)\nabla_y r\nabla_y^T r + I(\lambda+3\mu)\right] + O\left(r^0\right) \tag{33}$$

The fundamental solution of solid displacement $\hat{U}^s(r)$ can be dismantled into singular $\hat{U}_s^s(r)$ and regular $\hat{U}_r^s(r)$ parts as

$$\begin{aligned} \hat{U}^s(r) &= \hat{U}_s^s(r) + \hat{U}_r^s(r) \text{ with } r := |y-x| \\ &= \frac{1}{\mu}\left[I\Delta_y - \frac{\lambda+\mu}{\lambda+2\mu}\nabla_y\nabla_y^T\right]\Delta_y\hat{x}(r) \\ &\quad -\frac{1}{\mu}\left[\left(\left(k_1^2+k_2^2\right)\Delta_y - k_1^2k_2^2\right)I - \left(k_1^2+k_2^2-k_4^2-\frac{k_1^2k_2^2}{k_3^2}\right)\nabla_y\nabla_y^T\right]\hat{x}(r) \end{aligned} \tag{34}$$

in which

$$\begin{aligned} \hat{x}(r) &= \frac{1}{4\pi r}\left[\frac{e^{-k_1 r}}{(k_2^2-k_1^2)(k_3^2-k_1^2)} + \frac{e^{-k_2 r}}{(k_2^2-k_1^2)(k_2^2-k_3^2)} + \frac{e^{-k_3 r}}{(k_1^2-k_3^2)(k_2^2-k_3^2)}\right] \\ &= -\frac{1}{(k_1^2-k_2^2)(k_1^2-k_3^2)(k_3^2-k_2^2)} + O\left(r^2\right) \end{aligned} \tag{35}$$

The remaining parts of $\hat{U}(r)$ as in (30) can be described as [36].

$$\hat{U}^f(r) = \frac{\rho^f(\alpha-\beta)\nabla_y r}{4\pi r\beta(\lambda+2\mu)\left(k_1^2-k_2^2\right)}\left[\left(k_1+\frac{1}{r}\right)e^{-k_1 r}-\left(k_2+\frac{1}{r}\right)e^{-k_2 r}\right] = O\left(r^0\right) \quad (36)$$

$$\hat{P}^s(r) = \frac{\hat{U}^f(r)}{s} = O\left(r^0\right) \quad (37)$$

$$\hat{P}^f(r) = \frac{s\rho^f}{4\pi r\beta\left(k_1^2-k_2^2\right)}\left[\left(k_1^2-k_4^2\right)e^{-k_1 r}-\left(k_2^2-k_4^2\right)e^{-k_2 r}\right] = \frac{s\rho^f}{4\pi r\beta}+O\left(r^0\right) \quad (38)$$

On the basis of limiting process $\tilde{x}\in\Omega\to x\in\Gamma$ on (28) we get

$$\lim_{\tilde{x}\in\Omega\to x\in\Gamma}\left(\hat{V}\hat{t}^g\right)_\Omega(\tilde{x}) = \left(\hat{V}\hat{x}^g\right)(x) \coloneqq \dot{\int_\Gamma}\hat{U}^T(y-x)\hat{t}^g(y)ds_y \quad (39)$$

According to limiting process $\tilde{x}\in\Omega\to x\in\Gamma$ on (28) we obtain [42].

$$\lim_{\tilde{x}\in\Omega\to x\in\Gamma}\left(\hat{K}\hat{u}^g\right)_\Omega(\tilde{x}) = [-I(x)+C(x)]\hat{u}^g(x)+\left(\hat{K}\hat{u}^g\right)(x) \quad (40)$$

where

$$C(x) = \lim_{\varepsilon\to 0}\dot{\int_{y\in\Omega:|y-x|=\varepsilon}}\left(\hat{T}_y\hat{U}\right)^T(y-x)ds_y \quad (41)$$

and

$$\left(\hat{K}\hat{u}^g\right)(x) = \lim_{\varepsilon\to 0}\dot{\int_{|y-x|\geq\varepsilon}}\left(\hat{T}_y\hat{U}\right)^T(y-x)\hat{u}^g(y)ds_y \quad (42)$$

By using (39)-(42), we can write

$$C(x)\hat{u}^g(x) = \left(\hat{V}\hat{t}^g\right)(x)-\left(\hat{K}\hat{u}^g\right)(x) \quad (43)$$

By applying the inverse Laplace transform, we obtain

$$C(x)u^g(x,t) = (V*t^g)(x,t)-(Ku^g)(x,t) \quad (44)$$

where $*$ is the time convolution.
According to [40], the fundamental solution is

$$\left(\hat{T}_y\hat{U}\right)^T = \left[\begin{bmatrix}\hat{T}_y^e & san_y\\ -\beta n_y^T & \frac{\beta}{s\rho_0^f}n_y^T\nabla_y\end{bmatrix}\begin{bmatrix}\hat{U}^s & \hat{U}^f\\ \left(\hat{P}^s\right)^T & \hat{P}^f\end{bmatrix}\right]^T = \begin{bmatrix}\hat{T}^s & \hat{T}^f\\ \left(\hat{Q}^s\right)^T & \hat{Q}^f\end{bmatrix} \quad (45)$$

On the basis of Stokes theorem, we obtain

$$\dot{\int_\Gamma}(\nabla_y\times \mathrm{a}, n_y)ds_y = -\dot{\int_{\partial\Gamma}}(\mathrm{a}, v)d\gamma_y = -\dot{\int_\phi}(\mathrm{a}, v)d\gamma_y = 0 \quad (46)$$

which can be expressed as

$$\int_{\dot{\Gamma}} (n_y \times \nabla_y, \mathrm{a}) ds_y = 0 \tag{47}$$

On the basis of [40], we get

$$\int_{\dot{\Gamma}} (M_y\ \mathrm{a}) ds_y = 0 \tag{48}$$

in which $M_y = \left(\nabla_y \nabla_y^T\right)^T - \nabla_y \nabla_y^T$.
By applying (48) to a formula $\mathrm{a} = vu$ we obtain [43].

$$\int_{\dot{\Gamma}} (M_y\ v) u ds_y = -\int_{\dot{\Gamma}} v (M_y\ u) ds_y \tag{49}$$

$$\int_{\dot{\Gamma}} (M_y\ v)^T u ds_y = -\int_{\dot{\Gamma}} v^T (M_y\ u) ds_y \tag{50}$$

Making use of (34) and (45), we can express $\hat{T}^s$ as

$$\left(\hat{T}^s\right)^T = \left(T_y^e \left(\hat{U}^s{}_{sing} + \hat{U}^s_{reg}\right)\right)^T + s\alpha \hat{P}^s n_y^T = \left(T_y^e \hat{U}^s{}_{sing}\right)^T + O(r^0) \tag{51}$$

On the basis of [40], we obtain

$$\left(\hat{T}^s\right)^T = (\lambda + 2\mu) n_y \nabla_y^T \hat{U}^s{}_{sing} - \mu\left(n_y \times \left(\nabla_y \times \hat{U}^s{}_{sing}\right)\right) + 2\mu M_y \hat{u}^s{}_{sing} + O(r^0) \tag{52}$$

which may be expressed using (34) as

$$\left(\hat{T}^s\right)^T = M_y \Delta_y^2 \hat{X} + I\left(\mathrm{n}^T \nabla_y\right) \Delta_y^2 \hat{X} + 2\mu\left(M_y \hat{U}^s{}_{sing}\right)^T + o(r^0) \tag{53}$$

By applying (29) (53), we obtain

$$\left(\hat{k}\hat{u}\right)^s_{\Omega}(\tilde{x}) = \int_{\dot{\Gamma}} \left[\left(M_y \Delta_y^2 \hat{X}\right)\hat{u} + \left(I\left(\mathrm{n}^T \nabla_y\right) \Delta_y^2 \hat{X}\right)\hat{u} + 2\mu\left(M_y \hat{U}^s{}_{sing}\right)^T \hat{u} + o(r^0)\hat{u}\right] ds_y \tag{54}$$

Based on [42], we have

$$\left(\hat{K}\hat{u}\right)^s_{\Omega}(\tilde{x}) = \int_{\dot{\Gamma}} \left[-\Delta_y^2 \hat{X}\left(M_y \hat{u}\right) + \left(I\left(n^T \nabla_y\right) \Delta_y^2 \hat{X}\right)\hat{u} + 2\mu \hat{U}^s_s\left(M_y \hat{u}\right) + o(r^0)\hat{u}\right] ds_y \tag{55}$$

In the in right-side of (55), we can write second term as follows

$$\left(n^T \nabla_y\right) \Delta_y^2 \hat{x}(r) = \frac{n^T \nabla_y r}{4\pi r^2} + O(r^0) \tag{56}$$

in which

$$C^s(x) = I(x)\, c(x) \text{ with } c(x) = \frac{\phi(x)}{4\pi} \tag{57}$$

According to [40], we can write

$$\lim_{\Omega \in \tilde{x} \to x \in \Gamma} \left(\hat{K}\hat{u}\right)^s_{\Omega}(\tilde{x}) = -I(x)[-1 + c(x)]\hat{u}(x) + \left(\hat{K}\hat{u}\right)^s(x) \tag{58}$$

By augmenting $\hat{U}^s_s$ to $\hat{U}^s$, we obtain

$$\left(\hat{k}\hat{u}\right)^s_{\Omega}(\tilde{x}) = \int_{\Gamma} -\Delta^2_y \hat{x}\left(M_y \hat{u}\right) + \left(I\left(n^T \nabla_y\right)\Delta^2_y \hat{x}\right)\hat{u} + 2\mu \hat{U}^s\left(M_y \hat{u}\right) + O\left(r^0\right)\hat{u}\, ds_y \tag{59}$$

According to [41], we get

$$(f * g)(t) = \int_0^t f(t-\tau)g(\tau)d\tau \text{ for } t \in [0, T] \tag{60}$$

where

$$(f * g)(t_n) \approx \sum_{k=0}^{n} \omega^{\Delta t}_{n-k}\left(\hat{f}\right) g(t_k) \tag{61}$$

On the basis of Lubich [44, 45], the integration weights ω_n are calculated using Cauchy's integral formula as

$$\omega^{\Delta t}_{n-k}\left(\hat{f}\right) \coloneqq \frac{1}{2\pi i} \int_{|z|=R} \hat{f}\left(\frac{\gamma(z)}{\Delta t}\right) z^{-(n+1)} dz \tag{62}$$

Polar coordinate transformation $z = Re^{-i\varphi}$ is used with the trapezoidal rule to approximate the integral (62) as

$$\omega^{\Delta t}_n\left(\hat{f}\right) \approx \frac{R^{-1}}{L+1} \sum_{\ell=o}^{L} \hat{f}(s_\ell)\zeta^{\ell n} \quad \text{with } \zeta = e^{\frac{2\pi i}{L+1}} \text{ and } s_\ell = \frac{\gamma\left(R\zeta^{-\ell}\right)}{\Delta t} \tag{63}$$

Substitution of Eq. (63) into Eq. (61), we get

$$\begin{aligned}(f * g)(t_n) &\approx \sum_{k=0}^{N} \frac{R^{-(n-k)}}{N+1} \sum_{\ell=0}^{N} \hat{f}(s_\ell)\zeta^{\ell(n-k)} g(t_k) \\ &\approx \frac{R^{-n}}{N+1} \sum_{\ell=0}^{N} \hat{f}(s_\ell)\hat{g}(s_\ell)\zeta^{\ell n}\end{aligned} \tag{64}$$

with

$$\hat{g}(s_\ell) = \sum_{k=0}^{N} R^k g(t_k)\zeta^{-\ell k}. \tag{65}$$

According to the procedure [43], the convolution operator (44) can be expressed as

$$C(x)u^g(x,t) = (v * t^g)(x,t) - (k * u^g)(x,t) \tag{66}$$

which may be written as

$$C(x)\hat{u}^g(x,s_\ell) = \left(\hat{v}\hat{t}^g\right)(x,s_\ell) - \left(\hat{k}\hat{u}^g\right)(x,s_\ell), \quad \ell = 0 \ldots \ldots .. N \tag{67}$$

Let the boundary Γ is discretized into N_e boundary elements τ_e as follows

$$\Gamma \approx \Gamma_h = \bigcup_{e=1}^{N_e} \tau_e \tag{68}$$

Now, we assume that we have

$$S_h[k](\Gamma_{N,h}) \coloneqq span\left\{\varphi_i^\alpha[k]\right\}_{i=1}^{\mathbb{i}}, \quad \alpha \geq 1 \tag{69}$$

$$S_h[k](\Gamma_{D,h}) \coloneqq span\left\{\psi_i^\beta[k]\right\}_{j=1}^{\mathbb{j}}, \quad \beta \geq 0 \tag{70}$$

where

$$\hat{u}^g[k](x) \approx \hat{u}_h^g[k](x) = \sum_{i=1}^{\mathbb{i}} \hat{u}_{h,i}^g[k]\varphi_i^\alpha[k](x) \in S_h[k](\Gamma_{N,h}) \tag{71}$$

$$\hat{t}^g[k](x) \approx \hat{t}_h^g[k](x) = \sum_{j=1}^{\mathbb{j}} \hat{t}_{h,j}^g[k]\psi_j^\beta[k](x) \in S_h[k](\Gamma_{D,h}) \tag{72}$$

where $k = 1, 2, 3, 4$ are the poro-elastic degrees of freedom, $\varphi_i^\alpha[k]$ are $\mathbb{i}$ continuous polynomial shape functions and $\psi_i^\beta[k]$ are $\mathbb{j}$ piecewise discontinuous polynomial shape functions.

Thus, from (67), we can write the following $N+1$ algebraic systems of equations

$$\begin{bmatrix} \hat{V}_{DD} - \hat{K}_{DN} \\ \hat{V}_{ND} - \left(C + \hat{K}_{NN}\right) \end{bmatrix}_\ell \begin{bmatrix} \hat{t}_{D,h}^g \\ \hat{u}_{N,h}^g \end{bmatrix}_\ell = \begin{bmatrix} -\hat{V}_{DN} & \left(C + \hat{K}_{DD}\right) \\ -\hat{V}_{NN} & \hat{K}_{ND} \end{bmatrix}_\ell \begin{bmatrix} \hat{g}_{N,h}^g \\ \hat{g}_{D,h}^g \end{bmatrix}_\ell \quad \ell = 0 \ldots N \tag{73}$$

5. Numerical results and discussion

In the current study, a Krylov subspace iterative method is used for solving the resulting linear systems. In order to reduce the number of iterations, a dual threshold incomplete LU factorization technique (ILUT) which is one of the well-known preconditioning techniques is implemented as a robust preconditioner for TFQMR (Transpose-free quasi minimal residual) [46] to accelerate the convergence of the solver TFQMR.

To illustrate the numerical calculations computed by the proposed technique, the physical parameters for transversely isotropic soft tissue are given as follows [47]:

The elasticity tensor

$$C_{ablg} = \begin{bmatrix} C_{11} & C_{12} & C_{13} & 0 & 0 & 0 \\ C_{12} & C_{11} & C_{13} & 0 & 0 & 0 \\ C_{13} & C_{13} & C_{33} & 0 & 0 & 0 \\ 0 & 0 & 0 & C_{44} & 0 & 0 \\ 0 & 0 & 0 & 0 & C_{44} & 0 \\ 0 & 0 & 0 & 0 & 0 & C_{66} \end{bmatrix} \tag{74}$$

in which

$$\begin{aligned} C_{11} &= \frac{E^2 v_0^2 - EE_0}{(1+v)\left(2Ev_0^2 + E_0(v-1)\right)}, C_{12} = -\frac{E^2 v_0^2 + EE_0 v}{(1+v)\left(2Ev_0^2 + E_0(v-1)\right)} \\ C_{13} &= -\frac{EE_0 v}{2Ev_0^2 + E_0(v-1)}, C_{33} = -\frac{E_0^2(v-1)}{2Ev_0^2 + E_0(v-1)} \\ C_{44} &= \mu_0, \;\; C_{66} = \frac{1}{2}(C_{11} - C_{12}) \end{aligned} \tag{75}$$

where

$$v = 0.196, v_0 = 0.163, \mu_0 = 20.98 \text{ GPa}, E = 68.34 \text{ GPa}, E_0 = 51.35 \text{ GPa} \tag{76}$$

and therefore

$$k_1 = 108.39 \text{ GPa}, k_2 = -21.70 \text{ GPa} \tag{77}$$

where E and E_0 are the respectively, v and v_0 are Poisson's ratio in the isotropy plane and in the fiber direction respectively, and μ_0 is the shear moduli in any direction within a plane perpendicular to isotropy plane.

Since for strongly anisotropic soft tissue both bulk moduli are positive, we used the following physical parameters for anisotropic soft tissue [48].

$$v = 0.95, v_0 = 0.49, \mu_0 = 20.98 \text{ GPa}, E = 22 \text{ kPa}, E_0 = 447 \text{ kPa} \tag{78}$$

and therefore

$$k_1 = 1243 \text{ kPa}, k_2 = 442 \text{ kPa} \tag{79}$$

and other constants considered in the calculations are as follows.

$$\rho_s = 1600\, kg/m^3,\ \rho_{\mathcal{F}} = 1113\, kg/m^3, p = 25\, MPap = 25MPa,$$
$$\phi = 0.15 \text{ and } Q/R = 0.65. \tag{80}$$

The domain boundary of the current problem has been discretized into 21 boundary elements and 42 internal points as depicted in **Figure 2**. The computation was done using Matlab R2018a on a MacBook Pro with 2.9GHz quad-core Intel Core i7 processor and 16GB RAM.

Figure 3 shows the variation of the temperature T along x-axis for different values of fractional order parameter. It can be seen from this figure that the fractional order parameter has a significant influence on the temperature.

Figure 4 illustrates the variation of the displacement u_1 along x-axis for different values of fractional order parameter. It can be seen from this figure that the fractional order parameter has a significant influence on the displacement u_1.

Figure 5 shows the variation of the displacement u_2 along x-axis for different values of fractional order parameter. It can be seen from this figure that the fractional order parameter has a significant influence on the displacement u_2.

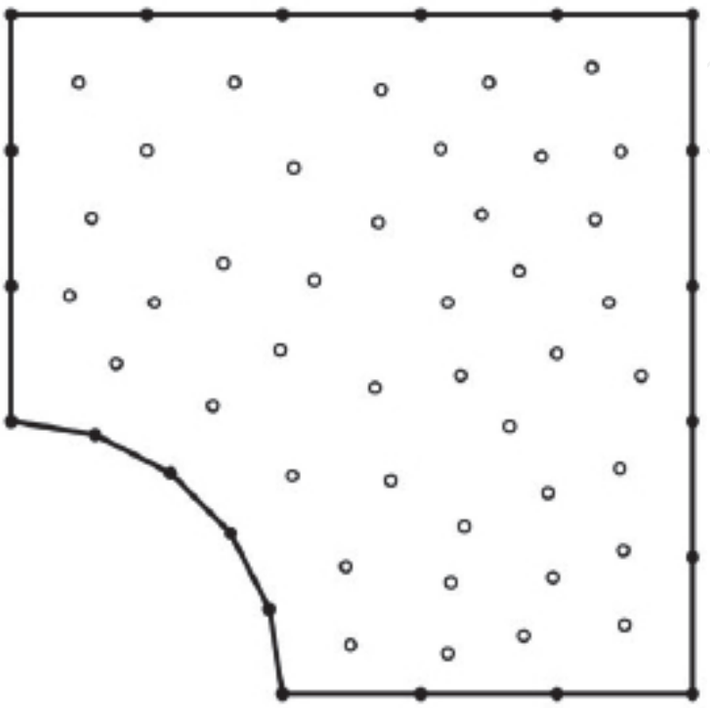

Figure 2.
Boundary element model of the current problem.

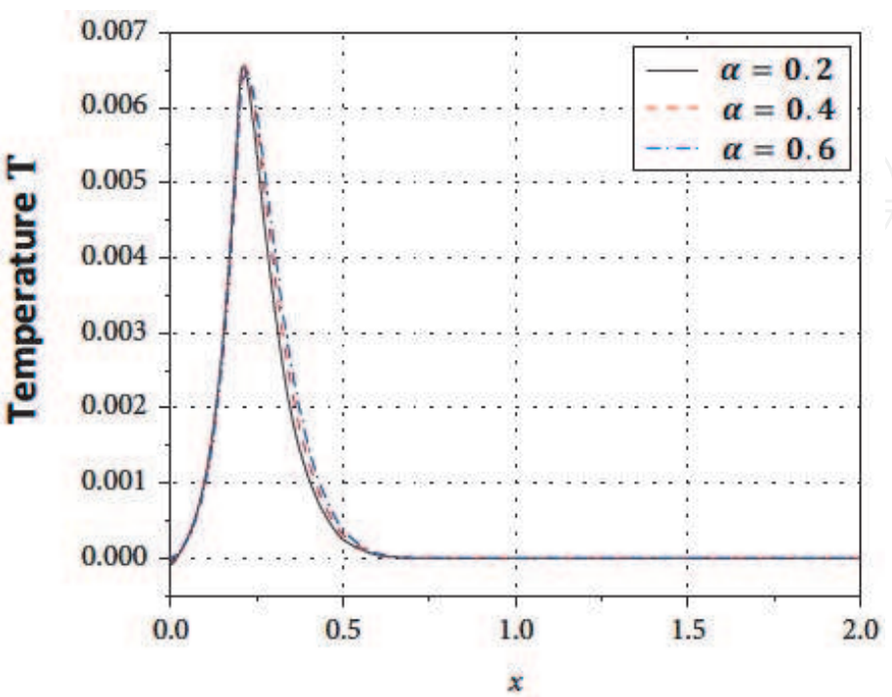

Figure 3.
*Variation of the temperature **T** along **x-axis**.*

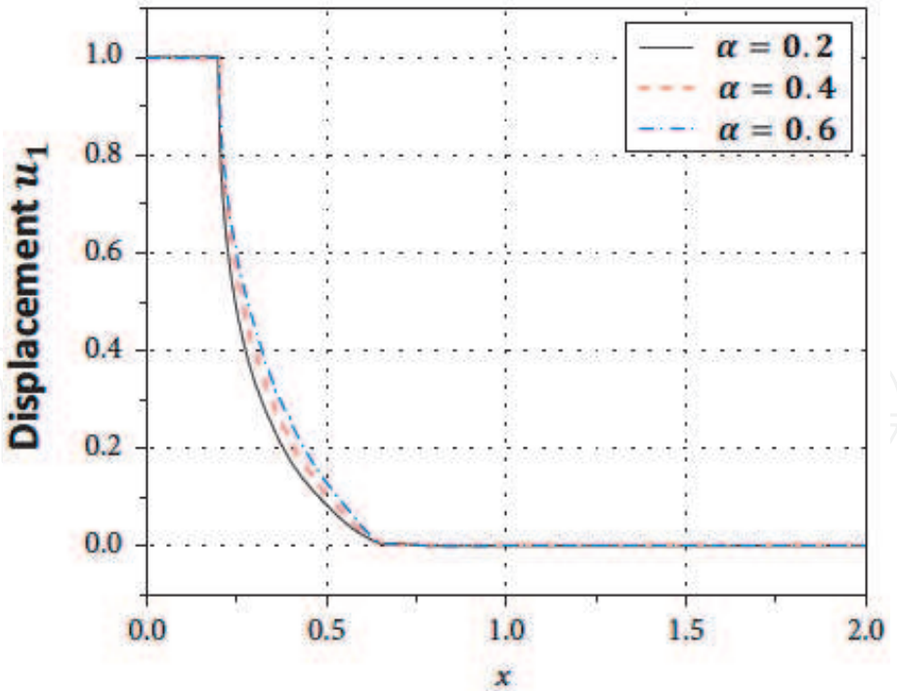

Figure 4.
*Variation of the displacement u_1 along **x-axis**.*

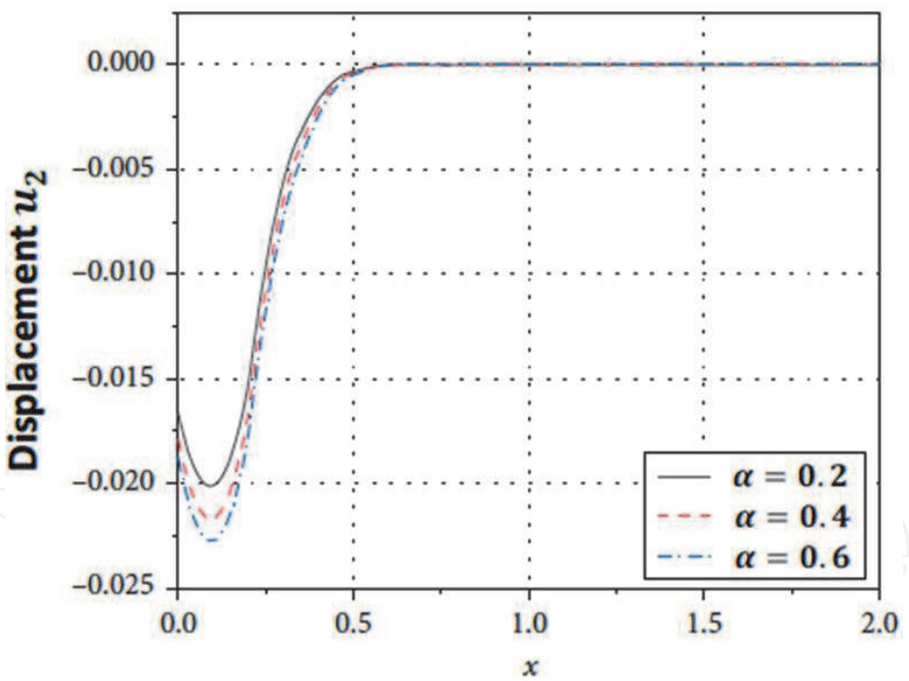

Figure 5.
*Variation of the displacement u_2 along **x-axis**.*

Figure 6 shows the variation of the fluid pressure p along x-axis for different values of fractional order parameter. It can be seen from this figure that the fractional order parameter has a significant influence on the fluid pressure p.

Figure 7 shows the variation of the bio-thermal stress σ_{11} along x-axis for different values of fractional order parameter. It can be seen from this figure that the fractional order parameter has an important influence on the bio-thermal stress σ_{11}.

Since there are no findings available for the problem under consideration. Therefore, some literatures may be regarded as special cases from our general problem. In the special case under consideration, the results of the bio-thermal

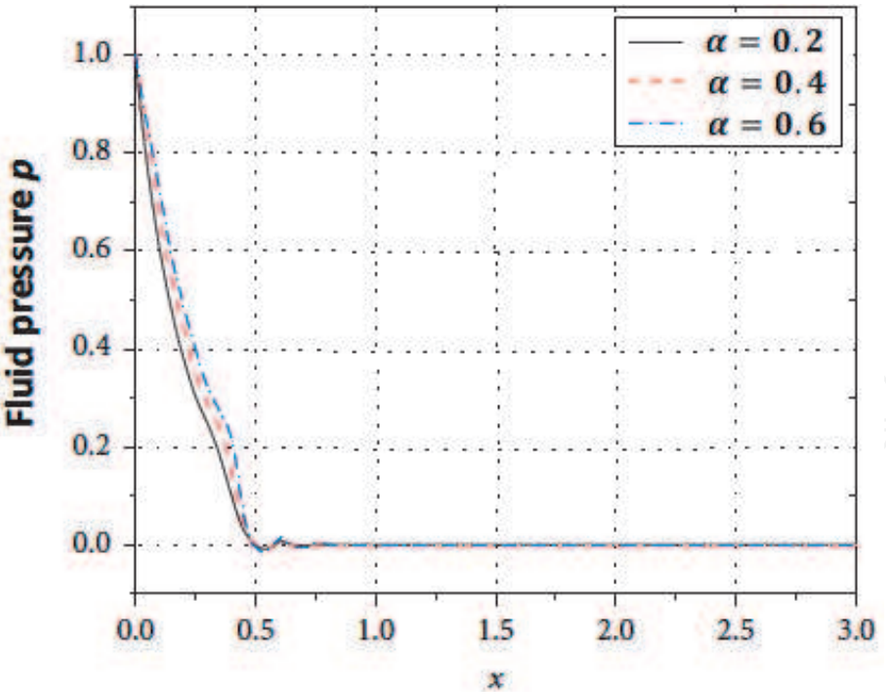

Figure 6.
Variation of the fluid pressure ***p*** *along* ***x-axis.***

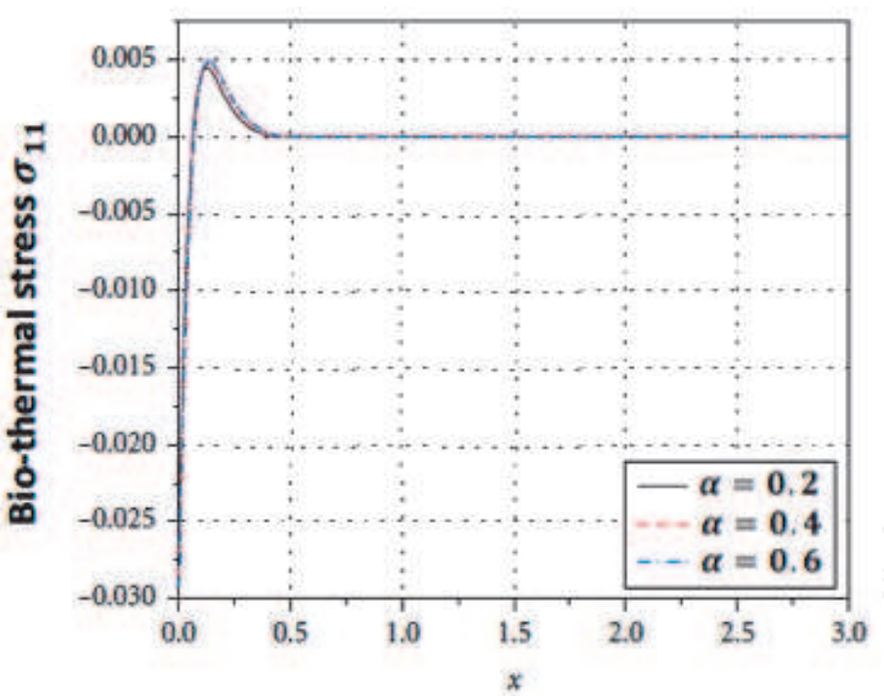

Figure 7.
Variation of the bio-thermal stress $\boldsymbol{\sigma_{11}}$ *along* ***x-axis.***

stress caused by coupling between the temperature and displacement fields are plotted in **Figure 8** to illustrate the variation of the bio-thermal stress σ_{11} along x-axis for BEM, FDM and FEM, where the boundary of the special case problem has been discretized into 21, 42 and 84 boundary elements (bes). The validity, accuracy and efficiency of our proposed technique have been confirmed by a graphical comparison of the three different boundary elements (21, 42 and 84) with those obtained using the FDM results of Shen and Zhang [49] and FEM results of Torvi and Dale [50] for the special case under consideration, the increase of BEM boundary elements leads to improve the accuracy and efficiency of the BEM, also, it can

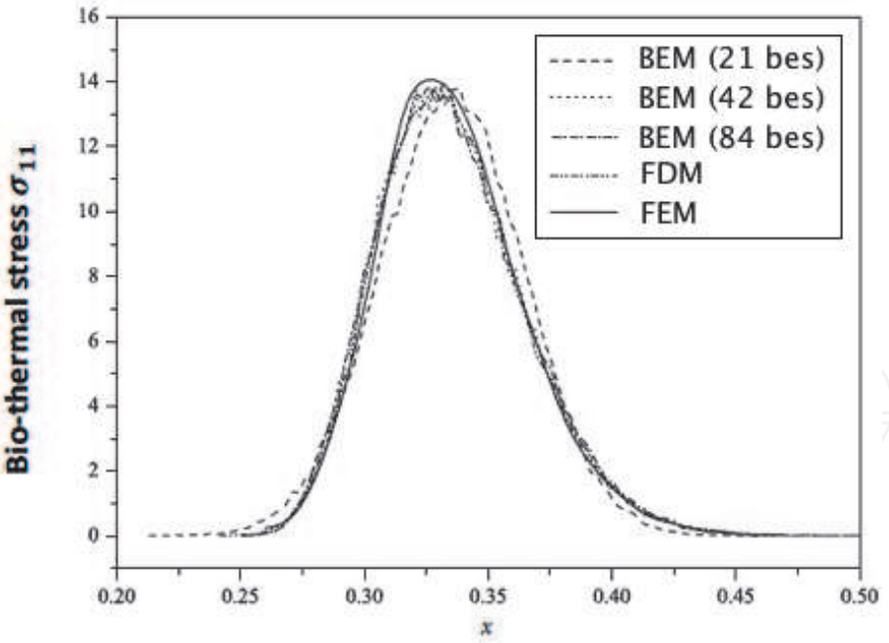

Figure 8.
*Variation of the bio-thermal stress σ_{11} along **x-axis** for BEM, FDM and FEM.*

be noted that the BEM findings are in excellent agreement with the FDM and FEM results, we refer the interested reader to recent work [51–55] for understanding the BEM methodology.

6. Conclusion

1. A novel boundary element model based on the TWMBT and Biot's theory was established for describing the bio-thermomechanical interactions in anisotropic soft tissues.

2. The bio-heat transfer equation has been solved using the dual reciprocity boundary element method (DRBEM) to obtain the temperature distribution.

3. The mechanical equation has been solved using the convolution quadrature boundary element method (CQBEM) to obtain the displacement and fluid pressure for different temperature distributions at each time step.

4. Due to the advantages of DRBEM and CQBEM such as dealing with more complex shapes of soft tissues and not needing the discretization of the internal domain, also, they have low RAM and CPU usage. Therefore, they are a versatile and powerful methods for modeling of fractional bio-thermomechanical problems in anisotropic soft tissues.

5. The linear systems resulting from BEM have been solved by TFQMR solver with the ILUT preconditioner which reduces the number of iterations and the total CPU time.

6. Numerical findings are presented graphically to show the effect of fractional order parameter on the problem variables temperature, displacements and fluid pressure.

7. Numerical findings confirm the validity, efficiency and accuracy of the proposed BEM technique.

8. The proposed technique can be applied to a wide variety of fractional bio-thermomechanical problems in anisotropic soft tissues.

9. For open boundary problems of soft tissues, such as the considered problem, the BEM users need only to deal with real geometry boundaries. But for these problems, FDM and FEM use artificial boundaries, which are far away from the real soft tissues. Also, these artificial boundaries are also becoming a big challenge for FDM users and FEM users. So, BEM becomes the best method for the considered problem.

10. The presence of fractional order parameter in the current study plays a significant role in all the physical quantities during modeling and simulation in medicine and healthcare.

11. From the research that has been performed, it is possible to conclude that the proposed BEM is an easier, effective, predictable, and stable technique in the treatment of the bio-thermomechanical soft tissue models.

12. It can be concluded from this chapter that Biot's equations for the dynamic response of poroelastic media can be combined with the bio-heat transfer models to describe the fractional bio-thermomechanical interactions of anisotropic soft tissues.

13. Current numerical results for our complex and general problem may provide interesting information for researchers and scientists in bioengineering, heat transfer, mechanics, neurophysiology, biology and clinicians.

Nomenclature

$A = \phi(1 + Q/R)$	Biot's coefficient
$B^e_{\tilde{x}}$	linear elastostatics operator
Γ	considered boundary
Γ_D	Dirichlet boundary
Γ_N	Neumann boundary
C	specific heat of soft tissue
$\mathbb{C}$	shape factor
C_b	specific heat of the blood
$C_{p\,jkl}$	specific heat of the blood
F	bulk body forces
$\hat{g}_D$	Dirichlet datum
$\hat{g}_N$	Neumann datum
K	dynamic permeability
$\mathcal{K}$	thermal conductivity of soft tissue
m	iterative parameter
p	pore pressure
$P_0(\tau)$	heating power
Q, R	solid–fluid coupling parameters
Q_{met}	metabolic heat source

Q_{ext}	external heat source
S_0	scattering coefficient
T	soft tissue temperature
$\breve{T}_b$	arterial blood temperature
T_x^e	traction derivative
u	solid displacement
u_f	fluid displacement
$V = V^f + V^s$	bulk volume
V^f	fluid volume
V^s	solid volume
W_b	blood perfusion rate
$\mathfrak{B}$	stress-temperature coefficients
$\in$	linear strain tensor
ζ	fluid volume variation
$\rho = \rho_s(1-\phi) + \phi\rho_f$	bulk density
$\rho_s = \mathbb{C}\phi\rho_f$	mass density of soft tissue
ρ_f	blood density
σ	total stress tensor
τ	time
τ_q	phase lag for heat flux
τ_T	phase lag for temperature gradient
$\varphi_i^\alpha[k]$	continuous polynomial shape functions
$\phi = \frac{V^f}{V}$	porosity
$\psi_j^\beta[k]$	discontinuous polynomial shape functions
Ω	considered region

Author details

Mohamed Abdelsabour Fahmy[1,2]

1 Jamoum University College, Umm Al-Qura University, Makkah, Saudi Arabia

2 Faculty of Computers and Informatics, Suez Canal University, Ismailia, Egypt

*Address all correspondence to: maselim@uqu.edu.sa; mohamed_fahmy@ci.suez.edu.eg

References

[1] Cho YI. Advances in Heat Transfer: Bioengineering Heat Transfer. San Diego: Academic Press Inc.; 1992

[2] Pennes HH. Analysis of tissue and arterial blood temperatures in the resting human forearm. J. Appl. Physiol. 1948;1:93–122.

[3] Askarizadeh H, Ahmadikia H. Analytical study on the transient heating of a two-dimensional skin tissue using parabolic and hyperbolic bioheat transfer equations. Appl. Math. Modell. 2015;39:3704–3720

[4] Li X., Li C., Xue Z., Tian X. Analytical study of transient thermo-mechanical responses of dual-layer skin tissue with variable thermal material properties. Int. J. Therm. Sci. 2018;124: 459–466

[5] Ahmadikia H., Fazlali R., Moradi A. Analytical solution of the parabolic and hyperbolic heat transfer equations with constant and transient heat flux conditions on skin tissue. Int. Commun. Heat Mass Transfer 2012;39:121–130.

[6] Shih TC, Yuan P, Lin WL, Kou HS. Analytical analysis of the Pennes bioheat transfer equation with sinusoidal heat flux condition on skin surface. Med. Eng. Phys. 2007;29:946–953.

[7] Lua WQ, Liub J, Zenga Y. Simulation of the thermal wave propagation in biological tissues by the dual reciprocity boundary element method. Eng. Anal. Boundary Elem. 1998;22:167–174.

[8] Shen W, Zhang J, Yang F. Modeling and numerical simulation of bioheat transfer and biomechanics in soft tissue. Math. Comput. Modell. 2005;41: 1251–1265.

[9] Zhang Y. Generalized dual-phase lag bioheat equations based on nonequilibrium heat transfer in living biological tissues. Int. J. Heat Mass Transfer 2009;52:4829–4834.

[10] Bourantas GC, Loukopoulos VC, Burganos VN, and Nikiforidis GC. A meshless point collocation treatment of transient bioheat problems. Int. J. Numer. Methods Biomed. Eng. 2014;30: 587–601

[11] Fahmy MA. A time-stepping DRBEM for the transient magneto-thermo-visco-elastic stresses in a rotating non-homogeneous anisotropic solid. Eng. Anal. Boundary Elem. 2012; 36:335–345.

[12] Fahmy MA. Transient magneto-thermoviscoelastic plane waves in a non-homogeneous anisotropic thick strip subjected to a moving heat source. Appl. Math. Modell. 2012;36:4565–4578.

[13] Fahmy MA. The effect of rotation and inhomogeneity on the transient magneto-thermoviscoelastic stresses in an anisotropic solid. ASME J. Appl. Mech. 2012;79:051015.

[14] Fahmy MA. Transient magneto-thermo-elastic stresses in an anisotropic viscoelastic solid with and without a moving heat source. Numer. Heat Transfer, Part A 2012;61:633–650.

[15] Fahmy MA. Implicit-Explicit time integration DRBEM for generalized magneto-thermoelasticity problems of rotating anisotropic viscoelastic functionally graded solids. Eng. Anal. Boundary Elem. 2013;37:107–115.

[16] Fahmy MA. Generalized magneto-thermo-viscoelastic problems of rotating functionally graded anisotropic plates by the dual reciprocity boundary element method. J. Therm. Stresses 2013;36:1–20.

[17] Fahmy MA. A three-dimensional generalized magneto-thermo-viscoelastic

problem of a rotating functionally graded anisotropic solids with and without energy dissipation. Numer. Heat Transfer, Part A 2013;63:713–733.

[18] Fahmy MA. Computerized boundary element solutions for thermoelastic problems: Applications to functionally graded anisotropic structures. Saarbrücken, Germany: LAP Lambert Academic Publishing; 2017.

[19] Fahmy MA. Boundary element computation of shape sensitivity and optimization: applications to functionally graded anisotropic structures. Saarbrücken, Germany: LAP Lambert Academic Publishing; 2017.

[20] Fahmy MA. Shape design sensitivity and optimization for two-temperature generalized magneto-thermoelastic problems using time-domain DRBEM. J. Therm. Stresses 2018;41:119–138.

[21] Fahmy MA. Shape design sensitivity and optimization of anisotropic functionally graded smart structures using bicubic B-splines DRBEM. Eng. Anal. Boundary Elem. 87 2018,87: 27–35.

[22] Pei RZ, Jing L, Cheng WC, Xue JP. Boundary element method (BEM) for solving normal or inverse bio-heat transfer problem of biological bodies with complex shape. J. Therm. Sci. 4 1995;4:117–124.

[23] Ooi EH, Ang WT, Ng EYK. A boundary element model for investigating the effects of eye tumor on the temperature distribution inside the human eye. Comput. Biol. Med. 2009; 39:667–677.

[24] Zhou J., Chen JK, Zhang Y. Simulation of Laser-Induced Thermotherapy Using a Dual-Reciprocity Boundary Element Model with Dynamic Tissue Properties. IEEE Trans. Biomed. Eng. 2010;57:238–245.

[25] Ng EYK, Tan HM, Ooi EH. Boundary element method with bioheat equation for skin burn injury. Burns 2009;35:987–997.

[26] Majchrzak E, Turchan L. The general boundary element method for 3D dual-phase lag model of bioheat transfer, Eng. Anal. Boundary Elem. 2015;50:76–82.

[27] Bottauscio O, Chiampi M, Zilberti L. Boundary Element Solution of Electromagnetic and Bioheat Equations for the Simulation of SAR and Temperature Increase in Biological Tissues. IEEE Trans. Magn. 2012;48: 691–694.

[28] Deng ZS, Liu J. Modeling of multidimensional freezing problem during cryosurgery by the dual reciprocity boundary element method. Eng. Anal. Boundary Elem. 2004;28:97–108

[29] Partridge PW, Wrobel LC. A coupled dual reciprocity BEM/genetic algorithm for identification of blood perfusion parameters. Int. J. Numer. Methods Heat Fluid Flow 2009;19:25–38.

[30] Chan CL. Boundary Element Method Analysis for the Bioheat Transfer Equation. J. Biomech. Eng. (1992;114:358–365.

[31] Wrobel LC. The boundary element method, Applications in thermos-fluids and acoustics. vol. 1. New York: Wiley; 2002.

[32] Wang CY, Achenbach JD. Elastodynamic fundamental solution for anisotropic solids. Geophys. J. Int. 1994; 118:384–392.

[33] Wang CY, Achenbach JD. Three-dimensional time-harmonic elastodynamic Green's functions for anisotropic solids. Proceedings of the Royal Society A: Mathematical, Physical and Engineering Sciences 1995;449: 441–458.

[34] Biot MA. Theory of propagation of elastic waves in a fluid- saturated porous solid. I. Low frequency range. J. Acoust. Soc. Am. 1956;28:168–178.

[35] Biot MA. Theory of propagation of elastic waves in a fluid- saturated porous solid. II. Higher frequency range. J. Acoust. Soc. Am. 1956;28:179–191.

[36] Schanz M. Wave propagation in viscoelastic and poroelastic continua. Lecture notes in applied mechanics. vol 2. New York: Springer; 2001.

[37] Xiaoyun Jiang and Haitao Qi, Thermal wave model of bioheat transfer with modified Riemann–Liouville fractional derivative, Journal of Physics A: Mathematical and Theoretical 2012; 45:485101

[38] Bonnet G, Auriault JL. Dynamics of saturated and deform- able porous media: homogenization theory and determination of the solid-liquid coupling coefficients. Physics of finely divided matter, Berlin: Springer Verlag; 1985. p. 306–316.

[39] Bonnet G. Basic singular solutions for a poroelastic medium in the dynamic range, J. Acoust. Soc. Am. 1987;82:1758–1763.

[40] Messner M, Schanz M. A regularized collocation boundary element method for linear poroelasticity. Comput. Mech. 2011;47:669–680.

[41] Fahmy MA. Boundary Element Modeling and Simulation of Biothermomechanical Behavior in Anisotropic Laser-Induced Tissue Hyperthermia. Engineering Analysis with Boundary Elements. 2019;101: 156–164. doi: 10.1016/j. enganabound.2019.01.006

[42] Steinbach O. Numerical approximation methods for elliptic boundary value problems. New York: Springer; 2008.

[43] Kielhorn L. A time-domain symmetric Galerkin BEM for viscoelastodynamics. In: Brenn G, Holzapfel GA, Schanz M, Steinbach O, eds. Computation in engineering and science. Austria: Graz University of Technology, Institute of Applied Mechanics; 2009.

[44] Lubich C. Convolution quadrature and discretized operational calculus. I. Numerische Mathematik 1988;52:129–145.

[45] Lubich C. Convolution quadrature and discretized operational calculus II. Numerische Mathematik 1988;52:413–425.

[46] Freund RW, Nachtigal NM. An implementation of the QMR method based on coupled two-term recurrences," SIAM J. Sci. Comput. 1994;15:313–337.

[47] Gilchrist MD, Murphy JG, Parnell W, Pierrat B. Modelling the slight compressibility of anisotropic soft tissue. Int. J. Solids Struct. 2014;51:3857–3865.

[48] Morrow DA, Haut Donahue TL, Odegard GM, Kaufman KR. Transversely isotropic tensile material properties of skeletal muscle tissue. J. Mech. Behav. Biomed. Mater. 2010;3: 124–129.

[49] Shen W, Zhang J. Modeling and numerical simulation of bioheat transfer and biomechanics in soft tissue. Math. Comput. Modell. 2005;41:1251–1265.

[50] Torvi DA, Dale JD. A finite element model of skin subjected to a flash fire. J. Biomech. Eng. 1994;116: 250–255.

[51] Fahmy MA, Shaw S, Mondal S, Abouelregal AE, Lotfy Kh., Kudinov IV, Soliman AH. Boundary Element Modeling for Simulation and Optimization of Three-Temperature Anisotropic Micropolar Magneto-

thermoviscoelastic Problems in Porous Smart Structures Using NURBS and Genetic Algorithm. International Journal of Thermophysics. 2021;42:29.

[52] Fahmy MA. A novel BEM for modeling and simulation of 3T nonlinear generalized anisotropic micropolar-thermoelasticity theory with memory dependent derivative. CMES-Computer Modeling in Engineering & Sciences. 2021;126:175–199.

[53] Fahmy MA. A new boundary element algorithm for modeling and simulation of nonlinear thermal stresses in micropolar FGA composites with temperature-dependent properties. Advanced Modeling and Simulation in Engineering Sciences. 2021 (In Press).

[54] Fahmy MA. A new BEM for fractional nonlinear generalized porothermoelastic wave propagation problems, Computers, Materials and Continua. 2021 (In Press).

[55] Fahmy MA. A new boundary element technique for one- and two-temperature models of biothermomechanical behavior of anisotropic biological tissues. 14th Virtual Congress WCCM & ECCOMAS 2020. Virtual congress 11–15 January 2021.